TÜBİTAK

Turkish Journal of Physics

http://journals.tubitak.gov.tr/physics/

Research Article

Turk J Phys
(2017) 41: 203 – 216

doi:10.3906/fiz-1610-24

Search of islands of stability for hypothetical superheavy nuclei using covariant density functional theory

Hazem ABUSARA[1,*], **Shakeb AHMAD**[2]
[1]Department of Physics, BirZeit University, Ramallah, Palestine
[2]Physics Section, Women's College, Aligarh Muslim University, Aligarh, India

Received: 26.10.2016 • **Accepted/Published Online:** 24.03.2017 • **Final Version:** 13.06.2017

Abstract: A systematic search for the location of islands of stability has been performed for the proton number $100 \leq Z \leq 220$ and the neutron number $Z + 30 \leq N \leq 2Z + 30$ using covariant density functional theory (CDFT), a relativistic Hartree–Bogoliubov (RHB) formalism with separable pairing, for two different force parameters, DD-ME2 and NL3*. Locations of the islands of stability are identified by analysis of the two-neutron and two-proton separation energy, two-nucleon shell gaps, vanishing neutron and proton pairing gap, energy surface, and the single particle states. The results show that beyond $^{292}120$ only Z = 154 and N > 220 can be a center of a new island of stability.

Key words: Density functional, superheavy nuclei

1. Introduction

Exploring the limit of the nuclear charge and mass is a driving force of research in nuclear structure studies. Thus nuclear structure studies of heavy and superheavy nuclei can be a starting point to extrapolate into the region far from the island of stability. Current experimental facilities are able to reach Z = 120, but theory should always lead the way for scientific advancement and to predict new phenomena.

The stability of a nucleus with very large proton number (Z $\geq$ 120) is mainly characterized by the shell effects. It is important to map the nuclear chart to find regions where the shell effects are strong enough to support the large numbers of protons. Thus one would expect that the self-consistent mean field methods will be the most successful methods for extrapolating into that region. However, there have been many studies that enriched our knowledge about superheavy nuclei using different models: Mic-Mac [1,2] and the covariant density functional [3–7]. In Ismail et al. [8] the framework of Strutinsky's approach is used and the authors cover a wide range of nuclei going into a region with a high number of protons including $72 \leq Z \leq 282$. Most of these studies focus their attentions on spherical shapes and perform all of the calculations. They make their predictions based on the assumption of spherical symmetry. Only recently, Agbemava et al. [9] reexamined the structure of superheavy nuclei, using deformed relativistic Hartree–Bogoliubov (RHB) formalism, where the authors predicted a greater role of the N = 184 neutron gap instead of the N = 172 neutron gap.

In this work, we explore the unknown territory of the nuclear landscape, characterized by an extremely high Z value, for the search of spherical shell closure that can be the center of an island of stability for the superheavy region. Our region of interest is defined by the proton number $100 \leq Z \leq 220$ and the neutron

*Correspondence: habusara@birzeit.edu

number $Z+30 \leq N \leq 2Z+30$. Our choice of this region, which include very large proton numbers, is similar to the region (but smaller) studied by Ismail et al. [8]. We perform both the spherical and deformed calculations to make sure that we indeed get spherical doubly magic nuclei.

The covariant density functional theory (CDFT) has been successful in describing many nuclear phenomena. It has been very successful in the description of the atomic nuclei behavior in extreme conditions such as high spin and deformation (super- and hyperdeformation) and it predicted that ^{107}Cd was the best candidate to observe discrete HD bands [10–13]. It was also used extensively in the description of fission barriers in actinides and superheavy regions of the nuclear chart. The average deviation between the calculated and experimental values of the height of the fission barrier in the actinide region was less than 1 MeV [14].

The manuscript is organized as follows. Section 2 provides a description of the covariant density functional theory in the RHB framework and the details of calculations. The results of spherical calculations are presented in section 3.1 and deformed results are discussed in section 3.2. A summary of the results and the conclusions are presented in section 4.

2. Theoretical formalism and details of calculations

In the CDFT the nucleus is described as a system of point-like nucleons, Dirac spinors, coupled to mesons and photons [15–17]. The nucleons interact by the exchange of several mesons, namely a scalar meson σ and three vector particles ω, ρ, and the photon. The starting point of the CDFT is a standard Lagrangian density [18]:

$$\begin{aligned} L = & \bar{\psi}\left(\gamma(i\partial - g_\omega\omega - g_\rho\vec{\rho}\vec{\tau} - eA) - m - g_\sigma\sigma\right)\psi \\ & + \frac{1}{2}(\partial\sigma)^2 - \frac{1}{2}m_\sigma^2\sigma^2 - \frac{1}{4}\Omega_{\mu\nu}\Omega^{\mu\nu} + \frac{1}{2}m_\omega^2\omega^2 \\ & - \frac{1}{4}\vec{R}_{\mu\nu}\vec{R}^{\mu\nu} + \frac{1}{2}m_\rho^2\vec{\rho}^2 - \frac{1}{4}F_{\mu\nu}F^{\mu\nu}, \end{aligned} \tag{1}$$

which contains nucleons described by the Dirac spinors ψ with the mass m and several effective mesons characterized by the quantum numbers of spin, parity, and isospin.

The Lagrangian (1) contains parameters as the meson masses m_σ, m_ω, and m_ρ and the coupling constants g_σ, g_ω, and g_ρ. e is the charge of the protons and it vanishes for neutrons. This model was first introduced by Walecka [17,19]. It turned out that the surface properties of finite nuclei cannot be described properly by this model. Therefore, Boguta and Bodmer [20] introduced density dependence via a nonlinear meson coupling replacing the term $\frac{1}{2}m_\sigma^2\sigma^2$ in Eq. (1) by

$$U(\sigma) = \frac{1}{2}m_\sigma^2\sigma^2 + \frac{1}{3}g_2\sigma^3 + \frac{1}{4}g_3\sigma^4. \tag{2}$$

The nonlinear meson nucleon coupling is represented by the parameter set NL3* [21] (see Table). Apart from the fixed values for the masses m, m_ω and m_ρ, there are six phenomenological parameters, m_σ, g_σ, g_ω, g_ρ, g_2, and g_3.

Moreover, one can introduce the density-dependent meson-nucleon coupling model that has an explicit density dependence for the meson-nucleon vertices. In this case there are no nonlinear terms in the σ meson, i.e. $g_2 = g_3 = 0$. The meson-nucleon vertices are defined as

$$g_i(\rho) = g_i(\rho_{sat})f_i(x) \text{ for } i = \sigma, \omega, \rho, \tag{3}$$

where the density dependence is given by

$$f_i(x) = a_i \frac{1 + b_i(x + d_i)^2}{1 + c_i(x + d_i)^2}. \tag{4}$$

for σ and ω and by

$$f_\rho(x) = \exp(-a_\rho(x - 1)) \tag{5}$$

for the ρ meson. x is defined as the ratio between the baryonic density ρ at a specific location and the baryonic density at saturation ρ_{sat} in the symmetric nuclear matter. The eight parameters in Eq. (4) are not independent but constrained as follows: $f_i(1) = 1$, $f_\sigma^{''}(1) = f_\omega^{''}(1)$, and $f_i^{''}(0) = 0$. These constraints reduce the number of independent parameters for density dependence to three. This model is represented in the present investigations by the parameter set DD-ME2 [22] given in the Table.

$$\left\{-\Delta + m_\sigma^2\right\}\sigma = -g_\sigma\rho_s - g_2\sigma^2 - g_3\sigma^3 \tag{6}$$

$$\left\{-\Delta + m_\omega^2\right\}\omega_\mu = g_\omega j^\mu \tag{7}$$

$$\left\{-\Delta + m_\rho^2\right\}\vec{\rho}_\mu = g_\rho\vec{j}^\mu \tag{8}$$

$$-\Delta A^\mu = e j_p^\mu \tag{9}$$

$$\hat{H}(r) = \sum_{i=1}^{A} \psi_i(r)^\dagger[\alpha p + \beta m]\psi_i(r) \tag{10}$$

$$+\frac{1}{2}[(\nabla\sigma)^2 + m_\sigma^2\sigma^2 + \frac{2}{3}g_2\sigma^3 + \frac{1}{2}g_3\sigma^4]$$

$$-\frac{1}{2}[(\nabla\omega)^2 + m_\omega^2\omega^2] - \frac{1}{2}[(\nabla\rho)^2 + m_\rho^2\rho^2]$$

$$+[g_\sigma\rho_s\sigma + g_\omega\gamma_\mu\omega^\mu + g_\rho\vec{j}_\mu\cdot\vec{\rho}_\mu + e j_{p\mu}A^\mu]$$

$$-\frac{1}{2}[(\nabla A)^2]$$

In the current investigation, the axially deformed RHB formalism with separable pairing model is used [23,24]. In the presence of pairing the single-particle density matrix is generalized to two densities [25]: the normal density $\hat{\rho}$ and the pairing tensor $\hat{k}$. The RHB model provides a unified description of particle-hole (ph) and particle-particle (pp) correlations on a mean-field level by using two average potentials: the self-consistent mean field that encloses all the long range ph correlations, and a pairing field $\hat{\Delta}$ that sums up the pp-correlations.

The ground state of a nucleus is described by a generalized Slater determinant, $|\Phi>$, that represents the vacuum with respect to independent quasiparticles. The quasiparticle operators are defined by the unitary Bogoliubov transformation of the single-nucleon creation and annihilation operators:

$$\alpha_k^+ = \sum_n U_{nk}c_n^+ + V_{nk}c_n \tag{11}$$

Table. NL3* and DD-ME2 parameterizations of the RMF Lagrangian.

Parameter	NL3*	DD-ME2
m	939	939
m_σ	502.5742	550.1238
m_ω	782.600	783.000
m_ρ	763.000	763.000
g_σ	10.0944	10.5396
g_ω	12.8065	13.0189
g_ρ	4.5748	3.6836
g_2	–10.8093	0.00000
g_3	–30.1486	0.00000
a_σ	0.00000	1.3881
b_σ	0.00000	1.0943
c_σ	0.00000	1.7057
d_σ	0.00000	0.4421
a_ω	0.00000	1.3892
b_ω	0.00000	0.9240
c_ω	0.00000	1.4620
d_ω	0.00000	0.4775
a_ρ	0.00000	0.5647

$$\hat{\rho}_{nn'} =< \Phi|c_n^+ c_{n'}|\Phi > \tag{12}$$

$$\hat{k}_{nn'} =< \Phi|c_n c_{n'}|\Phi > \tag{13}$$

The RHB energy density functional E_{RHB} is given by

$$E_{RHB}[\hat{\rho}, \hat{k}] = E_{RMF}[\hat{\rho}] + E_{pair}[\hat{k}] \tag{14}$$

$E_{RMF}[\hat{\rho}]$ is given by

$$E_{RMF}[\psi, \bar{\psi}, \sigma, \omega^\mu, \vec{\rho}^\mu, A^\mu] = \int d^3 r \hat{H}(r) \tag{15}$$

and the $E_{pair}[\hat{k}]$ is given by

$$E_{pair}[\hat{k}] = \tag{16}$$

$$= \frac{1}{4} \sum_{n_1 n_1'} \sum_{n_2 n_2'} k^*_{n_1 n_1'} < n_1 n_1' |V^{PP}| n_2 n_2' > k_{n_2 n_2'}$$

$< n_1 n_1' |V^{PP}| n_2 n_2' >$ are the matrix elements of the two-body pairing interaction.

$$V^{PP}(r_1, r_2, r_1', r_2') = -G\delta(R - R')P(r)P(r') \tag{17}$$

$$R = \frac{1}{\sqrt{2}}(r_1 + r_2)$$

$$r = \frac{1}{\sqrt{2}}(r_1 - r_2)$$

$$P(r) = \frac{1}{(4\pi a^2)^{3/2}} e^{-r^2/2a^2}$$

For details of the numerical derivation see Niksic et al. [24].

The CDFT equations are solved on the basis of an isotropic three-dimensional harmonic oscillator in Cartesian coordinates, with oscillator frequency $\hbar\omega_0 = 41A^{-1/3}$ MeV. For details see the literature [23,26]. The truncation of basis is performed in such a way that all states belonging to the shells up to fermionic $N_F = 20$ and bosonic $N_B = 20$ are taken into account. We consider only spherical symmetry, axial, and parity-conserving intrinsic states and solve the RHB equations in spherical and axially deformed oscillator basis [7,18,27,24].

The calculations are split into two parts. The first is with only spherical shape allowed; this will grant us the possibility of predicting shell closure based on the two-proton and two-neutron separation energy and will be done in Sec. 3.1. In the second part quadrupole deformation will be allowed, thus to test the candidates from the first part if they truly have a spherical shape at ground state and this will be done in Sec. 3.2.

We map the part of the nuclear chart specified with $100 \leq Z \leq 220$ and $Z + 30 \leq N \leq 2Z + 30$. Shell closures are identified with a large two-nucleon separation energy; thus as a first indicator of the shell closure we calculate the following quantities:

$$S_{2n}(N, Z) = B.E(N, Z) - B.E(N - 2, Z) \tag{18}$$

$$S_{2p}(N, Z) = B.E(N, Z) - B.E(N, Z - 2) \tag{19}$$

The two-nucleon shell gaps are defined as [28,29]

$$\delta_{2n}(N, Z) = S_{2n}(N + 2, Z) - S_{2n}(N, Z) \tag{20}$$

$$\delta_{2p}(N, Z) = S_{2p}(N, Z + 2) - S_{2p}(N, Z) \tag{21}$$

For the deformed calculations, the RHB framework is used. Binding energy as a function of deformation is studied for the nuclei nominated in the previous section to ensure their being doubly magic spherical nuclei.

The calculations are performed by imposing constraints on the axial mass quadrupole moments. The method of quadratic constraints uses a variation of the function

$$< \hat{H} > + C_{20}(\langle \hat{Q}_{20} \rangle - q_{20})^2, \tag{22}$$

where $< \hat{H} >$ is the total energy and $\langle \hat{Q}_{20} \rangle$ denotes the expectation values of the mass quadrupole operators

$$\hat{Q}_{20} = 2z^2 - x^2 - y^2 \tag{23}$$

In these equations, q_{20} is the constrained value of the multipole moment and C_{20} the corresponding stiffness constants [25].

3. Results

To completely identify a shell closure for the spherical nuclei, there are three conditions that must be satisfied [30] and similar to the approach in Ismail et al. [8]:

1. A peak in the two-nucleon shell gaps defined by Eqs. (20) and (21)
2. It is spherical ground state
3. Collapse of pairing at the spherical minimum

The first condition will be discussed in Sec. 3.1, while the other two will be discussed in Sec. 3.2

3.1. Spherical calculations

Systematic calculations of all even-even nuclei in the region defined by $100 \leq Z \leq 220$ and $Z+30 \leq N \leq 2Z+30$ are performed. Binding energy for every nucleus is obtained and the two-nucleon shell gap is calculated using Eqs. (20) and (21). The results are presented in Figures 1–8 using two parameterizations, NL3* and DD-ME2.

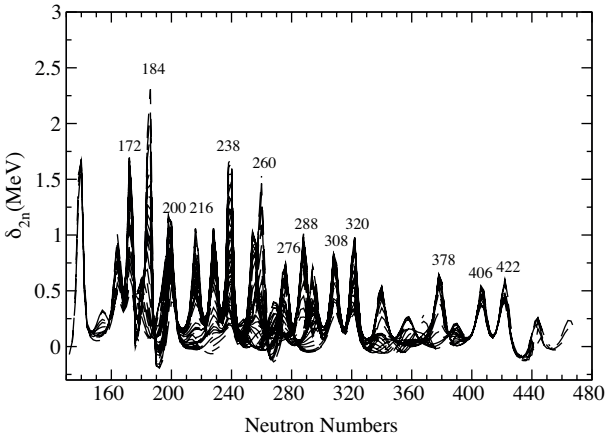

Figure 1. Two-neutron shell gap for different isotopic chains 100 < Z < 220, using NL3*.

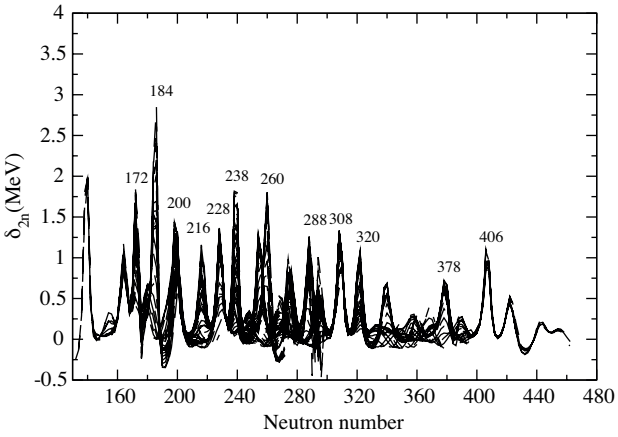

Figure 2. Same as Figure 1, but using DD-ME2.

The neutron candidates for magic numbers are shown in Figure 1. These candidates are divided into four categories based on the δ_{2n} values. The first one is N = 184, which has a value of 2.4 MeV, the highest among all the neutrons; thus it is the most favorable candidate for a magic number. The second category contains N = 238 and 260, which has around 1.5 MeV for δ_{2n}, which is comparable to that of the 172 gap, known to be the magic number in the CDFT; thus these numbers are also favorable due to their similarity to N = 172. The third category contains N = 200, 216, 276, 288, 308, and 320, which has a δ_{2n} value of around 1.1 MeV. The fourth group contains 378, 406, and 422, which are considered local peaks instead of global ones.

In Figure 3 one can see a color map of the δ_{2n} value of all the nuclei studied in this investigation and can clearly see that none of these candidates is dominant over the investigated region of the nuclear chart, but they are dominant locally. For example the N = 172 gap is mainly dominant between Z = 110 and 142 for the NL3* parametrization while for the DD-ME2 it is dominant for Z = 114–138, the N = 184 gap is dominant between Z = 100 and 128 for NL3* and between Z =100 and 130 for DD-ME2, and similar behavior can be seen for the other candidates; see Figure 3.

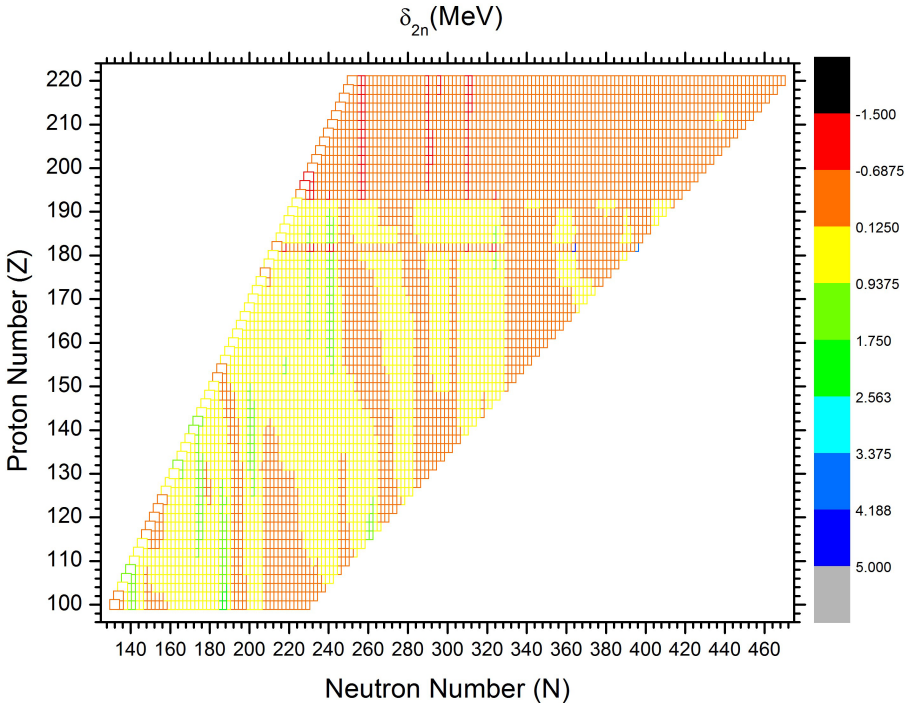

Figure 3. Two-neutron shell gap for all calculated nuclei using NL3*.

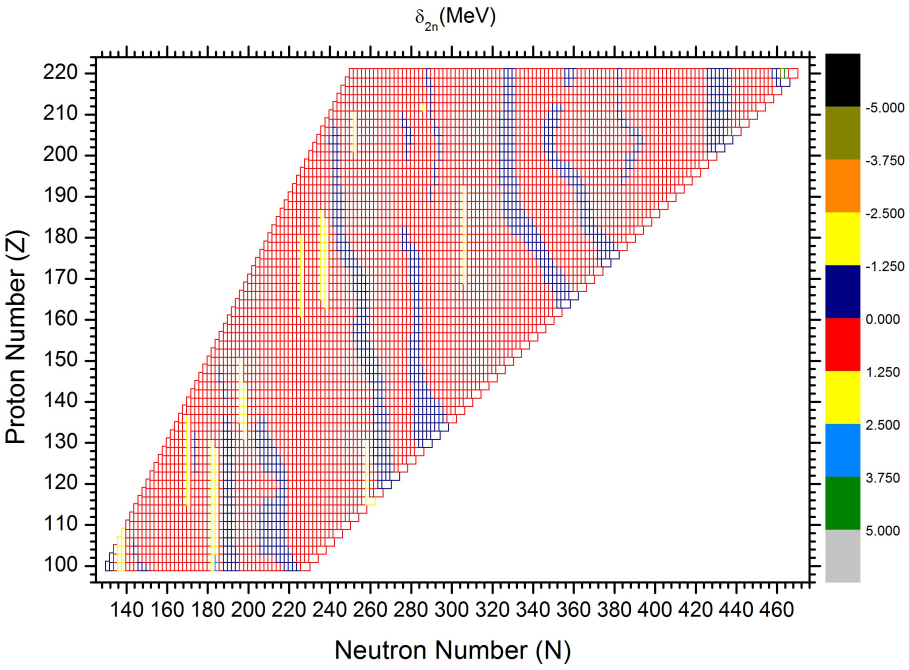

Figure 4. Two-neutron shell gap for all calculated nuclei using DD-ME2.

In a similar fashion, the proton magic number candidates are shown in Figures 5 and 6. The proton candidates can be divided into two categories; the first category contains Z = 154, which has around 3.0 MeV for δ_{2p}, which is comparable to that at Z = 120, known to be a magic number in the CDFT. Thus Z = 154 is

also favorable due to its similarity with Z = 120. The second category contains Z = 132, 138, 186, and 204, which has a δ_{2p} value of around 2.0 MeV. Thus we have a total of six protons candidates for the magic numbers. Contrary to the two-neutron shell gap the two-proton shell gap has a very strong dominance across the region under considerations. For instance the Z = 120 shell gap is well pronounced in almost all of the isotope chain, as can be seen in Figures 7 and 8. The other candidates behave similarly, as seen in these figures.

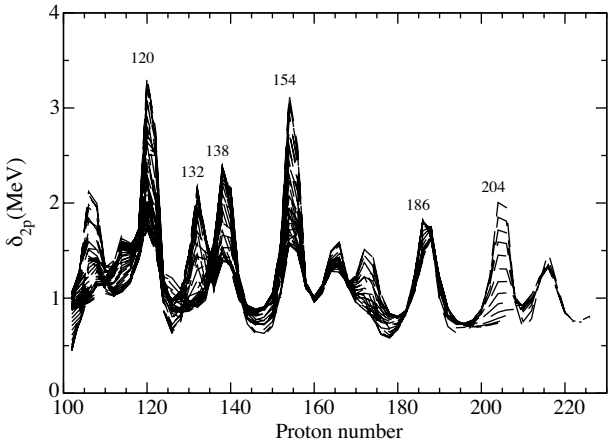

Figure 5. Two-proton shell gap using NL3*.

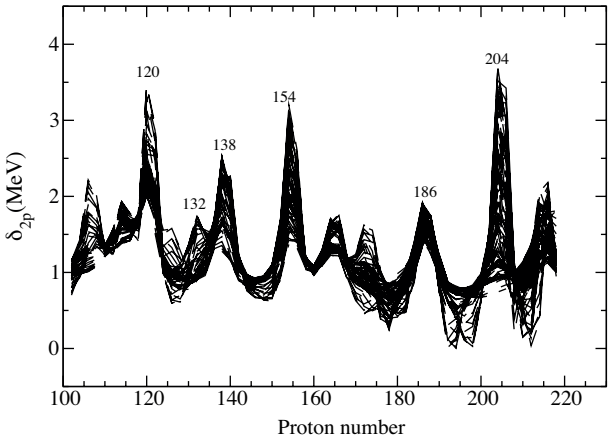

Figure 6. Same as Figure 5 but for DD-ME2.

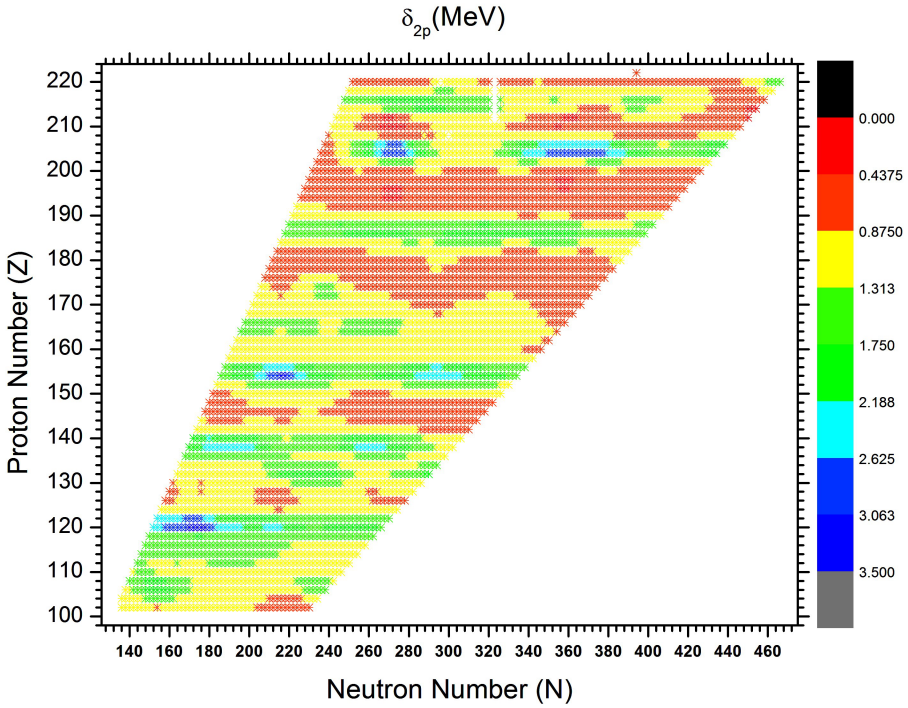

Figure 7. Two-proton shell gap for all calculated nuclei using NL3*.

The results are almost independent of parameterizations. For the neutron subsystem, as seen by comparing Figures 1 and 2, the predicted neutron magic numbers obtained in both parameterizations are identical except for N = 422. Moreover, the region of dominance of each magic number is reproduced in both of them; see Figures 3 and 4. Similarly, the proton subsystem results are reproduced exactly of same nature using both

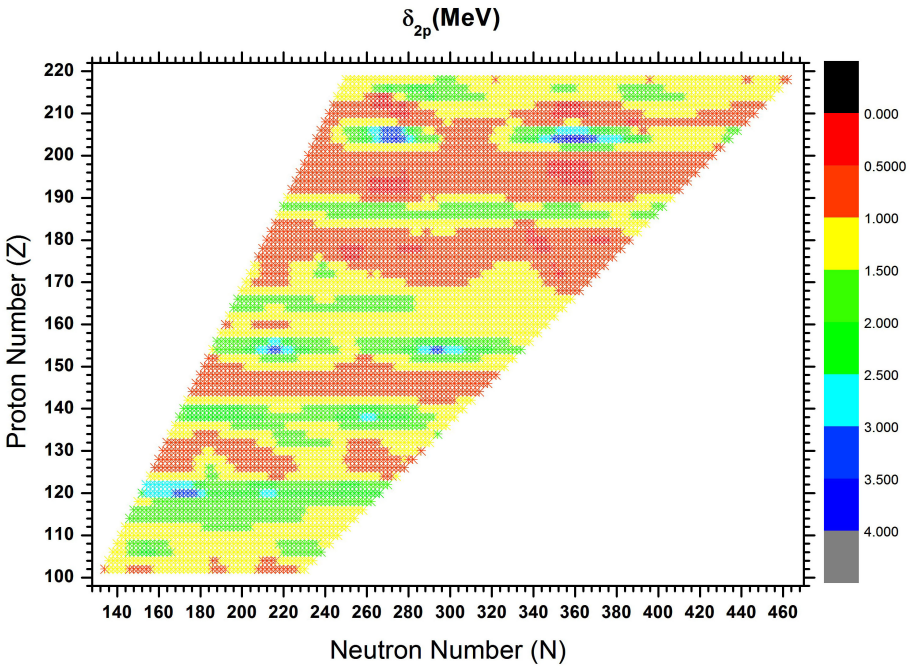

Figure 8. Two-proton shell gap for all calculated nuclei using DD-ME2.

parameterizations; the only difference is the enhancement of δ_{2p} for Z = 204 in DD-ME2 as compared with NL3*.

Our predictions are in partial agreement with the results obtained by Li et al. [6], where both of us predict a proton magic number at Z = 120, 138 and neutron magic number at N = 172, 184. In our case the nuclei that we nominate to be doubly magic are as follows:

Z = 120 and N = (292,304,320,336,348,358,380)

Z = 132 and N = (304,316,332,348,360,370,392,408,420)

Z = 138 and N = (310,322,338,354,366,376,398,414,426,446)

Z = 154 and N = (354,370,382,392,414,430,442,462,476)

Z = 186 and N = (402,414,424,446,462,474,494,508,540,546)

Z = 204 and N = (442,464,480,492,512,526,558,582,610)

Z = 216 and N = (454,476,492,504,524,538,570,594,622)

These results are also in good agreement with those reported by Ismail et al. [8]. It remains for us to check that these nuclei indeed have a spherical shape at ground state, which will be investigated in Sec. 3.2.

3.2. Deformed results

A spherical doubly magic nucleus must have a spherical shape at ground state. However, the results in Sec. 3.1 are based on the assumption that the nuclei under consideration are spherical. Thus we shall perform an additional check assuming that these nominated magic nuclei are having axial deformation. We performed the calculations on an axially deformed basis for all those nuclei nominated in the previous section, using two parameterizations, NL3* and DD-ME2. The result we got is the following nuclei $^{292}120$, $^{304}120$, $^{380}120$, $^{370}154$, $^{462}154$, and $^{476}154$, which have a spherical shape minimum. For these nuclei, the binding energy as a function

of β_2 deformation is presented in Figure 9 using both DD-ME2 and NL3* parameterizations. These nuclei belong to the two isotopic chains, Z = 120 and Z = 154.

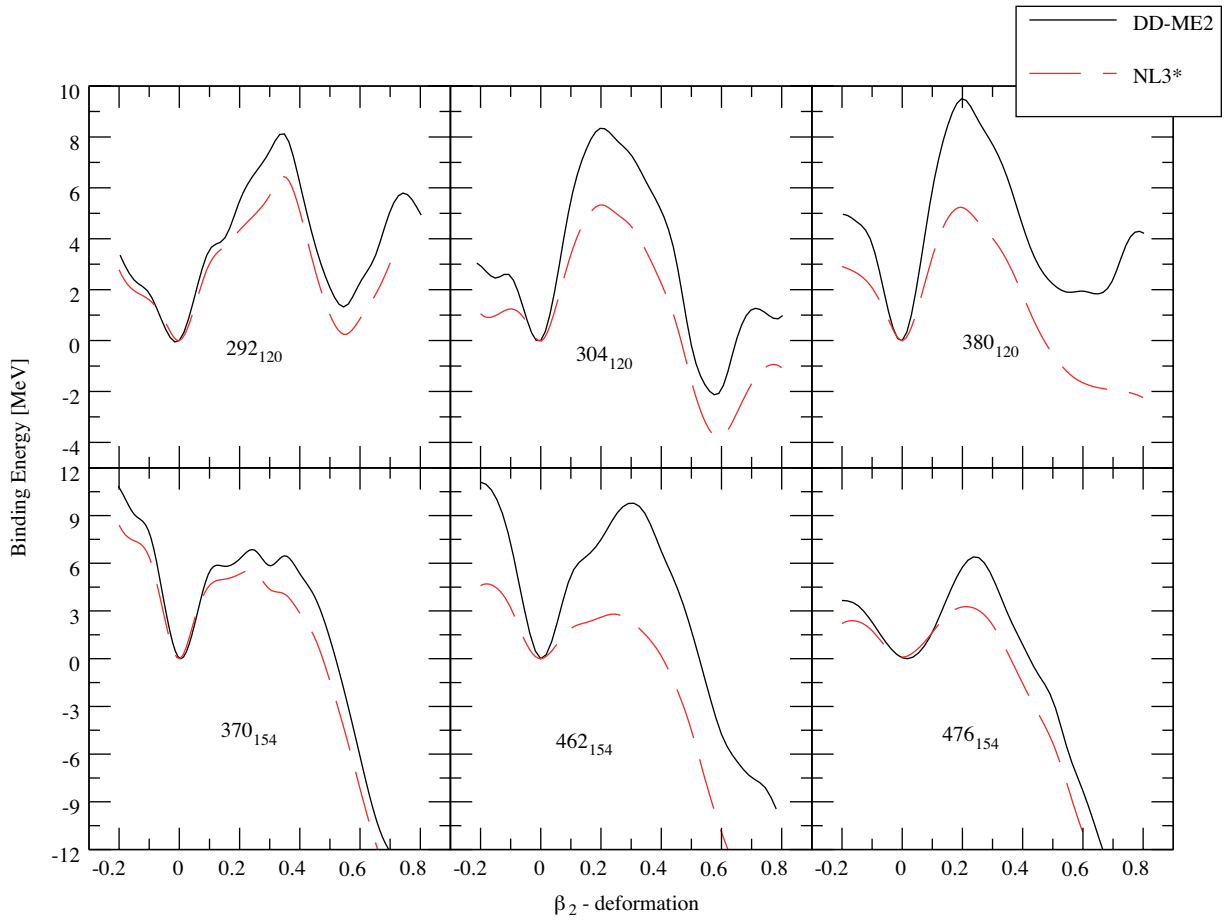

Figure 9. Binding energy as a function of quadrupole deformation (β_2) for $^{292}120$, $^{304}120$, $^{380}120$, $^{370}154$, $^{462}154$, and $^{467}154$ using two different parameterizations DD-ME2 and NL3*.

We can see that, for the Z = 120 isotopes, with DD-ME2 parameterization, the spherical minimum is followed by a barrier of around 10 MeV height, which increases the stability of these minima. However, as the number of neutrons increases, the spherical minimum becomes a local minimum, and another global minimum starts to form. For example the $^{304}120$ nucleus has a superdeformed minimum at $\beta_2 = 0.6$, which is followed by a smaller outer barrier as compared with the first inner barrier. According to Abusara et al. [31] the second outer barrier in the superheavy region of the nuclear chart is lowered by 2–3 MeV when one takes into account triaxiality and octupole deformation, while the inner barrier is not affected by either of them. Thus we can safely assume that the spherical minimum is indeed the ground state minimum for these nuclei. The conclusion remains the same with NL3* parameterization except the inner barrier height (6 MeV) here in this case is lower than the DD-ME2 parameterization.

The situation is different for the Z = 154 isotopes. There is only one barrier and after the barrier there is a deep valley, which would suggest that once the nucleus reaches the top of the barrier it will go into fission. The stability of these nuclei will then be characterized by the height of the barrier. For $^{370}154$ the height of the barrier is around 6 MeV, in both NL3* and DD-ME2 parameterizations. For $^{476}154$ the barrier height is

around 6 MeV in DD-ME2, while it is 3 MeV in NL3*. Although there is a discrepancy between DD-ME2 and NL3*, both of them agree on the spherical minimum and provide some kind of stability of the nucleus. However, the main concern shows up in the calculations of $^{462}154$, where in DD-ME2 the height of the barrier is about 9 MeV while it is around 1.5 MeV in NL3*; thus it is inconclusive to say that this nucleus is doubly magic, since the barrier height is almost nonexisting in NL3*. It is difficult to classify $^{462}154$ as a doubly magic nucleus, while its stability against fission is questionable with NL3*. However, for DD-ME2 parameterization, we can still nominate $^{462}154$ as a candidate for the spherical shell closure on the basis of its large barrier height and spherical ground state.

Now it remains to check our third condition, that is the collapse of paring does indeed occur for these candidates. The proton and neutron pairing energy are shown in Figure 10. According to Sil et al. [30] a closed shell must have a zero pairing energy. Thus we examine the pairing energy for our candidates as a function of β_2 deformation. Only two nuclei, $^{292}120$ and $^{370}154$, have a collapse of pairing at spherical shape, as can be seen in Figure 10.

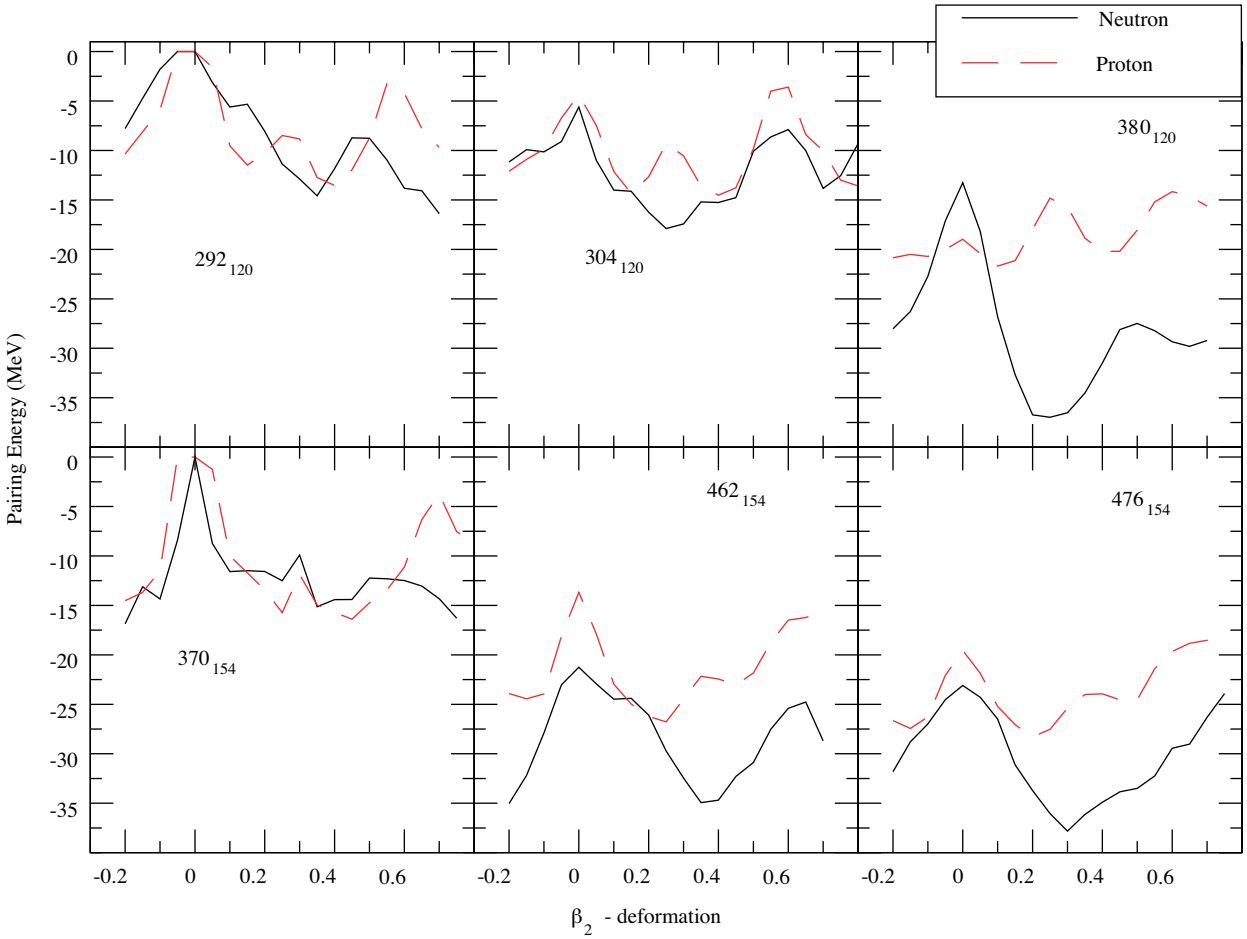

Figure 10. Pairing energy for $^{292}120$, $^{304}120$, $^{380}120$, $^{370}154$, $^{462}154$, and $^{467}154$.

Moreover, the density of the single particle states in the vicinity of the fermi level plays a major role in determining some properties of the nuclei. As an illustration, one can take a look at Figure 11 and can see the low density of the neutron single particle states near the fermi level for $^{292}120$. Look at the other nuclei that

are candidates of our search, $^{304}120$ and $^{380}120$, as shown in Figure 11. The level density increases with the neutron numbers as we move along the isotopic chain. Clearly, the nuclei become unbound as the number of neutrons increases beyond N = 160. This can be seen from the change in the location of the fermi level. It can be noted that as the number of neutron increases it reaches higher energy toward becoming unbound. Similarly, the single particle states for the proton as shown in Figure 12 show low density for the $^{292}120$ in the vicinity of the Fermi level, and that the density of the states increases with the neutron numbers as shown in Figure 12, but they still remain bound. Thus one can make a connection between the level density of the states and the shell closure of these nuclei. With lower density of the states one can expect the occurrence of shell closure.

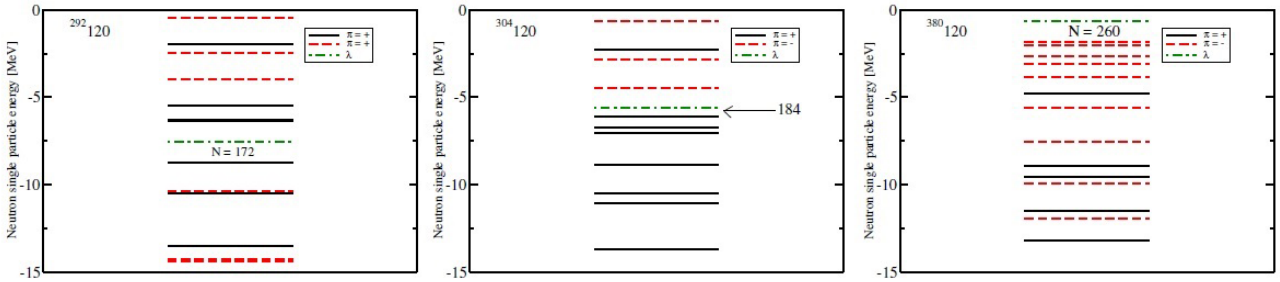

Figure 11. Neutron single particle states for $^{292,304,380}120$, λ is the chemical potential, using NL3*.

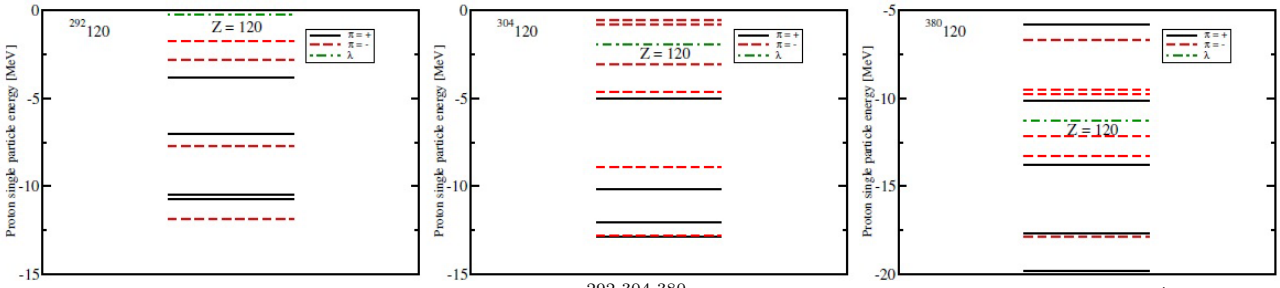

Figure 12. Proton single particle states for $^{292,304,380}120$, λ is the chemical potential, using NL3*.

One can do similar analysis for other three candidates that belong to the Z = 154 isotopic chain, but unfortunately our results indicated that the candidate nucleus $^{370}154$ is unbound. Thus, none of them is a possible candidate.

The vanishing of the pairing energy can be attributed to the density of the states near the fermi level. The pairing energy given by Eq. (16) and the two-body interaction depends on the creation and annihilation operator, exciting a nucleon into higher levels. The smaller the density of the states, the smaller the probability to contribute to the pairing energy.

4. Conclusions

We mapped the region located in $100 \leq Z \leq 220$, ($72 \leq Z \leq 282$ as in Ismail et al. [8]), with neutron number $Z + 30 \leq N \leq 2Z + 30$, using a RHB formalism with separable pairing for the spherical and deformed calculations. The force parameters used are the density dependent finite range interaction, i.e. DD-ME2 parameter, and nonlinear meson exchange interaction, i.e. NL3* parameter. We summarize the procedure and results as follows:

- The two-neutron separation energy and the two-proton separation energy were calculated using a spherical basis for all the nuclei in that region.
- Proton numbers and neutron numbers corresponding to the peaking of δ_{2p} and δ_{2n} were observed, respectively, and are considered as candidates for the center of new islands of stability.
- Nuclei that can be formed from proton and neutron numbers obtained using the spherical basis calculations were studied using the axially deformed basis calculations.
- On the basis of the potential energy surface study, for those nuclei that were found spherical in ground state, proton and neutron pairing energy were calculated. One expects collapse of the pairing for closed shells.
- Single particle states density is directly connected to both the shell closure and vanishing of the pairing energy.
- We predict that beyond Z = 120 it is very difficult to exactly identify a nucleus to be at the center of the new island of stability. However, we can predict that Z = 154 is a proton shell closure and one of the isotopes that has N $>$ 220 might be a center of the new island of stability.
- In future studies one has to take triaxiality into account. However, this will make the calculations time consuming and it will be discussed in a separate manuscript.
- The results are independent of the choice of parameterizations.

References

[1] Möller, P.; Nix, J. R.; Myers, W. D.; Swiatecki, W. J. *Atom. Data Nucl. Data* **1995**, *59*, 185-381.

[2] Baran, A.; Ojewski, Z. Ł.; Sieja, K.; Kowal, M. *Phys. Rev. C* **2005**, *72*, 044310.

[3] Rutz, K.; Bender, M.; Bürvenich, T.; Schilling, T.; Reinhard, P. G.; Maruhn, J. A.; Greiner, W. *Phys. Rev. C* **1997**, *56*, 238-243.

[4] Bender, M.; Rutz, K.; Reinhard, P. G.; Maruhn, J. A.; Greiner, W. *Phys. Rev. C* **1999**, *60*, 034304.

[5] Zhang, W.; Meng, J; Zhang, S. Q.; Geng, L. S.; Toki, H. *Nucl. Phys. A* **2005**, *753*, 106-135.

[6] Li, J. J.; Long, W. H.; Margueron, J.; Van Giai, N. *Phys. Lett. B* **2014**, *732*, 169-173.

[7] Agbemava, S. E.; Afanasjev, A. V.; Ray, D.; Ring, P. *Phys. Rev. C* **2014**, *89*, 054320.

[8] Ismail, M. A.; Ellithi, Y.; Adel, A; Anwer, H. *J. Phys. G: Nucl. Part. Phys.* **2016**, *43*, 015101.

[9] Agbemava, S. E.; Afanasjev, A. V.; Nakatsukasa, T.; Ring, P. *Phys. Rev. C* **2016**, *92*, 054310.

[10] Twin, P. J.; Nyakó, B. M.; Nelson, A. H.; Simpson, J.; Bently, M. A.; Cranmer-Gordon, H. W.; Forsyth, P. D.; Howe, D.; Mokhtar, A. R.; Morrison, J. D.; et al. *Phys. Rev. Lett.* **1986**, *57*, 811.

[11] Singh, B.; Zywina, R.; Firestone, R. B. *Nucl. Data Sheets* **2002**, *97*, 241.

[12] Afanasjev, A. V.; Abusara, H. *Phys. Rev. C* **2008**, *78*, 014315.

[13] Abusara, H.; Afanasjev, A. V. *Phys. Rev. C* **2009**, *79*, 024317.

[14] Abusara, H.; Afanasjev, A. V.; Ring, P. *Phys. Rev. C* **2010**, *82*, 044303.

[15] Reinhard, P. G. *Rep. Prog. Phys.* **1989**, *52*, 439.

[16] Vretenar, D.; Afanasjev, A. V.; Lalazissis, G.; Ring, P. *Phys. Rep.* **2005**, *409*, 101-259.

[17] Serot, B. D.; Walecka, J. D. *Adv. Nucl. Phys.* **1986**, *16*, 1.

[18] Gambhir, Y. K.; Ring, P.; Thimet, A. *Ann. Phys.-New York* **1990**, *198*, 132-179.

[19] Walecka, J. D. *Ann. Phys.-New York* **1974**, *83*, 491-529.

[20] Boguta, J.; Bodmer, A. R. *Nucl. Phys. A* **1977**, *292*, 413-428.

[21] Lalazissis, G. A.; Karatzikos, S.; Fossion, R.; Peña Arteaga, D.; Afanasjev, A. V.; Ring, P. *Phys. Lett. B* **2009**, *671*, 36-41.

[22] Lalazissis, G. A.; Nikšić, T.; Vretenar, D.; Ring, P. *Phys. Rev. C* **2005**, *71*, 024312.

[23] Koepf, W.; Ring, P. *Nucl. Phys. A* **1989**, *493*, 61-82.

[24] Niksic, T.; Paar, N.; Vretenar, D.; Ring, P. *Comp. Phys. Comm.* **2014**, *185*, 1808-1821.

[25] Ring, P.; Schunck, P. *The Nuclear Many-Body Problem*; Springer-Verlag: Berlin, Germany, 1980.

[26] Afanasjev, A. V.; König, J.; Ring, P. *Nucl. Phys.* A **1996**, *608*, 107-242.

[27] Ring, P.; Gambhir, Y. K.; Lalazissis, G. A. *Comp. Phys. Comm.* **1997**, *105*, 77-97.

[28] Hofmann, S.; Ninov, V.; Heßberger, F. P.; Armbruster, P.; Folger, H.; Münzenberg, G.; Schött, H. J.; Popeko, A. G.; Yeremin, A. V.; Saro, S. et al. *Z. Phys. A-Hadron Nucl.* **1996**, *354*, 229-230.

[29] Oganessian, Yu. Ts.; Utyonkov, V. K.; Lobanov, Yu. V.; Abdullin, F. Sh.; Polyakov, A. N.; Shirokovsky, I. V.; Tsyganov, Yu. S.; Gulbekian, G. G.; Bogomolov, S. L.; Gikal, B. N.; et al. *Phys. Rev. Lett.* **1999**, *83*, 3154-3157.

[30] Sil, T.; Patra, S. K.; Sharma, B. K.; Centelles, M.; Viñas, X. *Phys. Rev. C* **2004**, *69*, 044315.

[31] Abusara, H.; Afanasjev, A. V.; Ring, P. *Phys. Rev. C* **2012**, *85*, 024314.